Vessel Orientation Constrained Quantitative Susceptibility Mapping (QSM) Reconstruction

Suheyla Cetin[1(✉)], Berkin Bilgic[2], Audrey Fan[3], Samantha Holdsworth[3], and Gozde Unal[4]

[1] Faculty of Engineering and Natural Sciences, Sabanci University, Istanbul, Turkey
suheylacetin@sabanciuniv.edu
[2] Athinoula A. Martinos Center for Biomedical Imaging, Charlestown, USA
berkin@nmr.mgh.harvard.edu
[3] Department of Radiology, Stanford University, Stanford, USA
{auddie,sjhold}@stanford.edu
[4] Department of Computer Engineering, Istanbul Technical University, Istanbul, Turkey
gozde.unal@itu.edu.tr

Abstract. QSM is used to estimate the underlying tissue magnetic susceptibility and oxygen saturation in veins. This paper presents vessel orientation as a new regularization term to improve the accuracy of l_1 regularized QSM reconstruction in cerebral veins. For that purpose, the vessel tree is first extracted from an initial QSM reconstruction. In a second step, the vascular geometric prior is incorporated through an orthogonality constraint into the QSM reconstruction. Using a multi-orientation QSM acquisition as gold standard, we show that the QSM reconstruction obtained with the vessel anatomy prior provides up to 40 % RMSE reduction relative to the baseline l_1 regularizer approach. We also demonstrate in vivo OEF maps along venous veins based on segmentations from QSM. The utility of the proposed method is further supported by inclusion of a separate MRI venography scan to introduce more detailed vessel orientation information into the reconstruction, which provides significant improvement in vessel conspicuity.

Keywords: QSM · Susceptibility MRI · QSM reconstruction · Vessel orientation constraint

1 Introduction

Susceptibility MRI provides exquisite contrast of the venous vasculature due to the presence of paramagnetic deoxyhemoglobin molecules in cerebral veins. Although susceptibility-weighted imaging has gained popularity due to its ability to depict the veins in clinical applications such as stroke and traumatic brain injury [1], this method suffers from non-local and orientation-dependent effects that may preclude accurate identification of brain vessels.

S. Ourselin et al. (Eds.): MICCAI 2016, Part III, LNCS 9902, pp. 467–474, 2016.
DOI: 10.1007/978-3-319-46726-9_54

As an alternative, vessel segmentation can be performed directly on QSM derived from MRI phase images [2]. Because dipolar field patterns have been deconvolved during QSM reconstruction, segmentation of vasculature on QSM images is expected to outperform magnitude- or phase- based approaches. Automated vessel detection may also provide anatomical priors to improve quantification of brain physiology from QSM, including oxygen extraction fraction (OEF) in cerebral veins. Baseline OEF is an important physiological parameter for tissue health in normal brain function and many cerebrovascular diseases [3]. Reliable estimation of OEF depends on robust and accurate QSM reconstruction within venous structures.

In this study, we present a new regularization constraint to the existing l_1-norm regularized QSM reconstruction [4,5]. The new regularization constraint incorporates prior information about the vessel anatomy and the orientation. The vessel orientation prior is estimated by extracting the vessel tree. This process uses high order vessel tractography on the QSM data itself or on separate angiography images [2].

2 Method

2.1 Segmentation

To extract a brain vessel tree from a given QSM or angiographic image volume, we utilized a recent framework based on a higher order tensor vessel tractography by [2,6]. The method in [2] involves a unified mathematical formulation which models the n-furcations, i.e. bifurcations or higher order junctions in vessel trees, jointly with tubular sections. A general Cartesian tensor is embedded into a 4-dimensional space so that antipodal asymmetries in Y-junction-like situations, which are abundant in vascular trees, can be accurately modeled. Starting from a few seed points (e.g. 5–6), an entire cerebral vein tree can be captured from the QSM by this technique, which provides the vessel orientation, its centerline (central lumen line), its thickness (vessel lumen diameter), locations of branching points, and lengths of branches. The extracted knowledge of centerlines permits OEF computation [7] along the vasculature. The only interaction to the method is providing seed points which lends itself to a simple practical vessel extraction process. The computation time for segmentation of the whole vessel tree is on the order of minutes (<10 min).

2.2 l_1-regularized QSM Reconstruction

To quantify oxygenation along brain vessels requires recovery of the underlying tissue susceptibility distribution from MRI observations of magnetic field perturbations. Tissue susceptibility χ is related to the measured field map ϕ via the formulation $\mathbf{DF}\chi = \mathbf{F}\phi$, where $\mathbf{F}$ is the Fourier transform operator and $\mathbf{D} = 1/3 - k_z^2/k^2$ is the susceptibility kernel in k-space. Due to the presence of zeros on the conical surface along the magic angle in this kernel, the solution of this system necessitates additional regularization.

Most popular types of existing QSM reconstruction techniques can be formulated by penalizing l_1-norm of gradients in three dimensions [5], and can be expressed as an unconstrained convex optimization problem, minimizing

$$\underset{\chi}{argmin}\ \frac{1}{2}\left\|\mathbf{F}^{-1}\mathbf{D}\mathbf{F}\chi-\phi\right\|_2^2+\alpha\cdot\left\|\mathbf{G}\chi\right\|_1 \tag{1}$$

where α is the regularization parameter and $\mathbf{G}=[\mathbf{G}_x;\mathbf{G}_y;\mathbf{G}_z]$ is the gradient operator in three spatial directions.

2.3 l_1-regularized QSM Reconstruction with Vessel Orientation (VO) Constraint

We propose a new regularization term to be added to Eq. 1. As a regularizer, we use the dot product between the $\mathbf{G}\chi$ and the orientation vector $\mathbf{V}=[\mathbf{V}_x;\mathbf{V}_y;\mathbf{V}_z]\in\mathbb{R}^3$. The new regularization term incorporates prior information about the vessel anatomy and the orientation. We expect OEF (and thus susceptibility) along the vessel direction to be relatively smooth. Thus, the $\mathbf{G}\chi$ inside a vessel should be orthogonal to the $\mathbf{V}$, and the dot product between $\mathbf{G}\chi$ and $\mathbf{V}$ should be small. The final constraint is weighted by a dilated vessel mask $\mathbf{M}$: $\left\|\mathbf{M}(\mathbf{G}\cdot\mathbf{V})\chi\right\|_1$, where the structuring element in the dilation is a cylinder and the size of its radius is the half of the vessel radius. Over each cross section of the vessel along the centerline, $\mathbf{V}$ is defined at each voxel as the difference between two consecutive centerline points. Then, $\mathbf{V}$ is weighted by a smooth surface which enhances it along the edges and suppresses along the centerline of the vessel and outside of $\mathbf{M}$.

Hence, the l_1-regularized and vessel orientation constrained reconstruction problem reads as:

$$\underset{\chi}{argmin}\ \frac{1}{2}\left\|\mathbf{F}^{-1}\mathbf{D}\mathbf{F}\chi-\phi\right\|^2+\alpha\cdot\left\|\mathbf{G}\chi\right\|_1+\lambda\left\|\mathbf{M}(\mathbf{G}\cdot\mathbf{V})\chi\right\|_1 \tag{2}$$

where α and λ are the regularization parameters. We perform the optimization by non-linear conjugate gradient with backtracking line-search using 200 iterations [8].

3 Experimental Results

In this section, we will show the results of the l_1-regularized QSM reconstruction with vessel orientation (VO) constraint on: (Sect. 3.1) a ground truth in vivo validation data; (Sect. 3.2) in vivo QSM volumes acquired on ten healthy volunteers; (Sect. 3.3) a single in vivo QSM volume registered with a contrast-enhanced Fast Spin Echo MRI (MFAST) data. The regularization parameters (α, λ) were determined by parameter sweeping based on the validation data. The values ($\alpha=8.3\cdot10^{-4}$, $\lambda=3.5\cdot10^{-2}$) that minimized the normalized root mean square error (RMSE) relative to the true χ were selected to be the optimal setting, and applied in all experiments.

3.1 Validation Data

A ground truth in vivo QSM dataset is obtained using 3D-Gradient Echo (GRE) acquisition at 12 different head orientations relative to the main magnetic field. Since the dipole kernel **D** varies as a function of the angle between the subject's head and the main field, an overdetermined system can be formed using data from multiple orientations to mitigate the ill-conditioning of dipole inversion. This technique is termed Calculation Of Susceptibility through Multiple Orientation Sampling (COSMOS), and obviates the need for additional regularization [9] to provide ground-truth quality susceptibility maps. For this acquisition, a healthy volunteer (female, age 30) was scanned with a 32-channel head coil on a Siemens 3T Trio system using TR/TE = 35/25 ms at 1 mm isotropic resolution with BW = 100 Hz/pixel upon 15-fold acceleration with the Wave-CAIPI sequence [10]. Raw phase images were processed using Laplacian unwrapping [11] and SHARP background removal [12] to yield tissue phase images from each orientation, which were jointly inverted to provide the COSMOS χ solution. Using the COSMOS reconstruction as the ground truth χ map (Fig. 1(a)), the field map ϕ was simulated using the forward dipole model $\phi = \mathbf{F}^{-1}\mathbf{DF}$, and Gaussian noise ($\sigma = 0.01$) was added.

Starting from the noisy field map (Fig. 1(b)), l_1-reconstruction results in 8.37 % RMSE which is calculated in the whole volume (Fig. 1(c)). We segmented the vessel tree from the χ map using the higher order tensor based vessel extraction method described in Sect. 2.1. Figure 1(d) depicts the extracted vessel tree, where 7 seed points are selected for the segmentation. l_1 regularized reconstruction with VO constraint has RMSE error of 5.13 % for the overall data (Fig. 1(e)). The results show that the improvement in the accuracy of the reconstruction with our vessel orientation constraint over the existing l_1 reconstruction is 40 % along the whole data. Qualitatively, it can be observed that smaller vessels are more visible in the reconstructions regularized with the additional VO constraint (Fig. 1(e)).

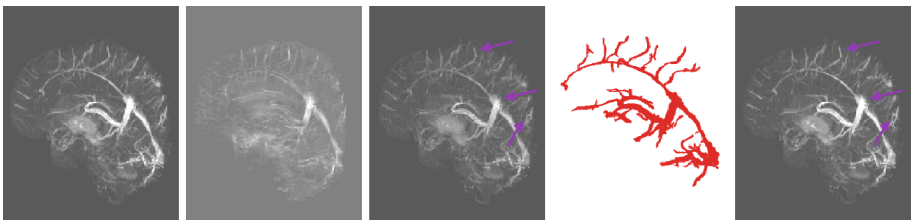

Fig. 1. Simulations result from ground truth susceptibility phantom. (a) Original χ field; (b) noisy normalized field map (input to QSM reconstruction); (c) l_1 regularized reconstructed χ field (8.37 % RMSE); (d) the extracted vessel tree (7 seed points are selected); (e) l_1 regularized reconstructed with VO constraint χ field (5.13 % RMSE). Arrows point out the reconstruction comparisons on the sample veins.

3.2 3D-GRE Volunteer Data

Ten young, healthy volunteers were scanned with a 32-channel coil on a Siemens 3T Trio system. 3D-GRE in vivo images for susceptibility mapping were acquired with full flow-compensation along each axis at all echoes. Axial magnitude and phase images were collected with TR = 23 ms; TE = 7.2/17.7 ms; resolution = $0.875 \times 0.875 \times 1\,\text{mm}^3$, matrix = $226 \times 256 \times 144$; and BW = 260 Hz/pixel. Phase images were combined offline and processed with Laplacian unwrapping [11]. Background field was removed with SHARP filtering [12] and QSM reconstruction was performed with a l_1 regularized reconstruction technique [4].

Figure 2 depicts the QSM map, centerlines and surfaces of the vessel trees on two healthy volumes. We compute the OEF values [7] after the l_1 regularized reconstruction with VO constraint on the same subjects. Mean OEF across all veins are $33.3 \pm 4\,\%$, $35.7 \pm 7\,\%$, $31.7 \pm 3\,\%$, $38.6 \pm 5\,\%$, $37.4 \pm 6\,\%$, $33.8 \pm 3\,\%$, $33.7 \pm 2\,\%$, $35.7 \pm 5\,\%$, $31.9 \pm 4\,\%$, and $34.3 \pm 9\,\%$ respectively, for each of ten subjects. Estimated OEF for straight sinus, sagittal sinus, pial vessels are $46.3 \pm 6\,\%$, $36.4 \pm 4\,\%$, $31.8 \pm 3\,\%$, respectively, in average of ten subjects. Furthermore, we display the OEF values on the vessel surfaces of the sample two subjects, where the VO constraint is shown to improve conspicuity of smaller vessels (Fig. 3).

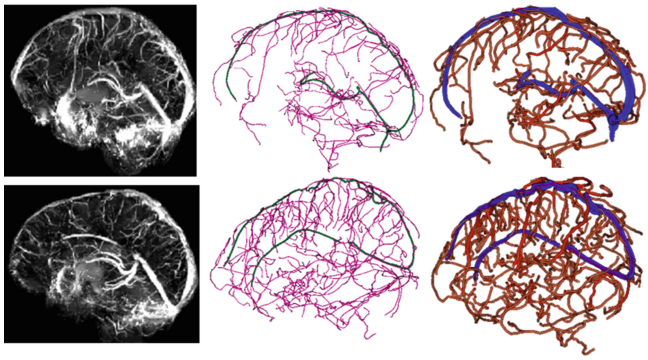

Fig. 2. (Left) original QSM map; (Middle) extracted centerlines of the vessels; (Right) surface renderings for the vessels are shown for two healthy subjects.

3.3 QSM + MFAST Data

The approach in Sect. 3.2 first uses standard QSM reconstruction (generic prior) and segments the vessels from this initial estimate of susceptibility. Here we test the hypothesis that vessel tree extraction from a separate angiographic volume offers improved vascular priors for OEF quantification from QSM maps.

With IRB approval, patients were scanned on a 3T GE scanner (MR750, GE Healthcare Systems, Waukesha, WI) with an 8-channel head-coil. A flow compensated 3D parallel-imaging-accelerated multi-echo (ME)-GRE sequence

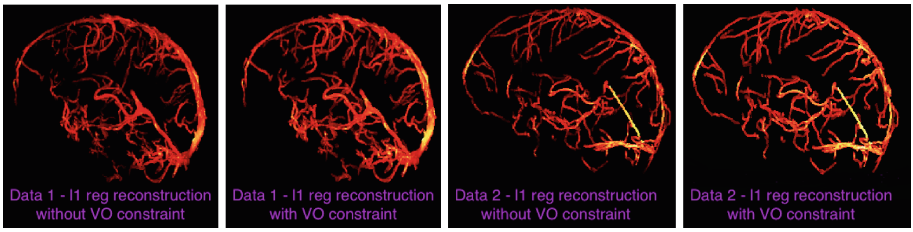

Fig. 3. OEF visualization on two sample subjects from ten data volume (shown in hot colors); l_1 regularized QSM reconstruction without (a, c) and with (b, d) VO constraint for the two subjects respectively.

was used with the following parameters: Axial plane, FOV = 22 cm, matrix size = 384×256, number of partitions = 66, resolution = $0.6 \times 0.9 \times 2\,\text{mm}^3$, acceleration factor = 2, flip angle = 15°, TR = 36 ms, seven echoes ranging from TE = 4 ms−33 ms (4.8 ms increments), scan time = 5.44 min. On completion of the scan, the raw data from the scanner were automatically reconstructed using compiled threaded MATLAB (MathWorks Inc., Natick, MA, USA) code.

A ferumoxytol-enhanced MRA using 3D SPGR was designed with short repetition time (TR) = 4 ms and echo time (TE) = 1 ms. The sequence was fat suppressed with FOV = 26 cm, matrix size = 416×416, resolution = $0.625 \times 0.625\,\text{mm}^2$ and 180 slices with 1 mm thickness. The excitation was done with a flip angle of 15 degrees, and receiver bandwidth of 62.5 kHz. The scan time was reduced by not acquiring the corners of ky-kz space, producing an acquisition time of 5.46 min.

We first extracted the brain using FSL [13] from MFAST data, then registered MFAST and QSM data with a rigid registration using the MedInria software [14]. Using the QSM reconstruction as the reference χ map, the field map ϕ was simulated using the forward dipole model, and Gaussian noise was added ($\sigma = 0.02$). Then, we segmented the vessel tree from QSM data and MFAST data separately. Figure 4 (Top) shows the vessel tree segmentation from QSM and MFAST data, respectively. We use morphological operators to separate veins from arteries for the MFAST data. Figure 4 (Bottom) visualizes the results of: (Left) QSM reconstruction without the vessel orientation prior; (Middle) QSM reconstruction with the vessel orientation prior where the vessel tree is segmented from the QSM data; (Right) QSM reconstruction with the vessel orientation prior where the vessel tree is segmented from the MFAST data. The results show the enhancements along the veins using our VO prior in the reconstructions. The amount of detail captured in the vessel tree extracted from the MFAST data volume, which is then incorporated into the QSM reconstruction through the VO regularizer clearly reveals the benefits of the new regularizer term.

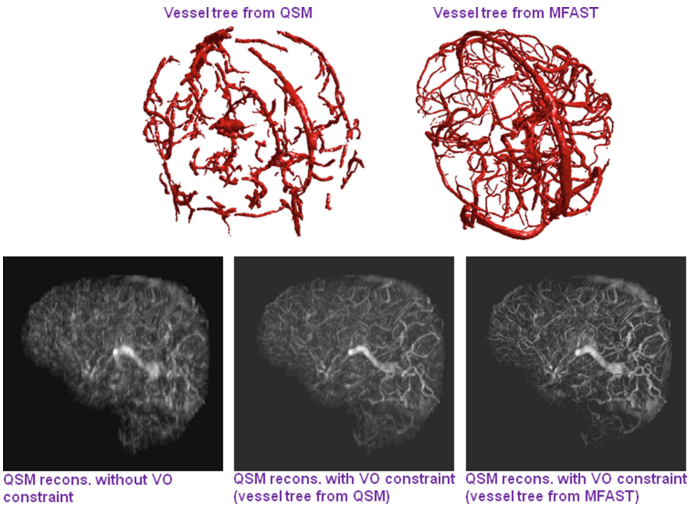

Fig. 4. Top: Left-vessel tree extraction from QSM data (Extr. 1), Right-vessel tree extraction from MFAST data (Extr. 2); Bottom: (Left) QSM reconstruction without VO, (Middle) l_1-reg QSM data reconstructed with VO constraint (Extr. 1), (Right) l_1-reg QSM data reconstructed with VO constraint (Extr. 2).

4 Conclusion

We developed a method that improves the accuracy of l_1 regularized QSM reconstruction [4,5] with a new regularization constraint, vessel orientation. Quantitative performance of our method was demonstrated on a ground truth phantom data. Furthermore, we performed the experiments on ten QSM images reconstructed from MRI phase and presented the mean OEF results for all veins in each volume and major vessel segments. On two sample subjects, we showed that the OEF maps along the vessel direction are relatively smooth. Finally, we compared the QSM reconstructions on a QSM volume acquired with an additional contrast, the MFAST. We showed the results for QSM reconstructions with and without vessel orientations where the vessel trees were segmented from QSM and MFAST data respectively. This experiment implied that when the segmentation becomes more detailed and accurate, the quality of the reconstruction increases. Use of the vessel orientation constraint increased OEF values (Fig. 3), such that our results are more in line with physiological OEF values reported by O-15 PET imaging [15]. This observation suggests that the use of anatomical prior helps mitigate partial volume effects and over-smoothing associated with traditional regularized QSM reconstruction. The new OEF values may also reflect less underestimation due to vessel orientation because of the vascular prior. In future work we will pursue the idea of extracting the vessel prior from the enhanced QSM image and iterating the whole procedure a few times which can lead to an improvement. We will also monitor both the number of vessel branches and OEF values over iteration number.

References

1. Hammond, K.E., Lupo, J.M., Xu, D., Veeraraghavan, S., Lee, H., Kincaid, A., Vigneron, D.B., Manley, G.T., Nelson, S.J., Mukherjee, P.: Microbleed detection in traumatic brain injury at 3T and 7T: comparing 2D and 3D gradient-recalled echo (GRE) imaging with susceptibility-weighted imaging (SWI). In: ISMRM, p. 248 (2009)
2. Cetin, S., Unal, G.: A higher-order tensor vessel tractography for segmentation of vascular structures. IEEE TMI **34**(10), 2172–2185 (2015)
3. Christen, T., Bolar, D.S., Zaharchuk, G.: Imaging brain oxygenation with mri using blood oxygenation approaches: methods, validation, and clinical applications. Am. J. Neuroradiol. **34**, 1113–1123 (2012)
4. Bilgic, B., Fan, A.P., Polimeni, J.R., Cauley, S.F., Bianciardi, M., Adalsteinsson, E., Wald, L.L., Setsompop, K.: Fast quantitative susceptibility mapping with l1-regularization and automatic parameter selection. MRM **72**(5), 1444–1459 (2014)
5. de Rochefort, L., Liu, T., Kressler, B., Liu, J., Spincemaille, P., Lebon, V., Wu, J., Wang, Y.: Quantitative susceptibility map reconstruction from MR phase data using bayesian regularization: validation and application to brain imaging. MRM **63**(1), 194–206 (2010)
6. Cetin, S., Demir, A., Yezzi, A.J., Degertekin, M., Unal, G.: Vessel tractography using an intensity based tensor model with branch detection. IEEE TMI **32**(2), 348–363 (2013)
7. Fan, A.P., Bilgic, B., Gagnon, L., Witzel, T., Bhat, H., Rosen, B.R., Adalsteinsson, E.: Quantitative oxygenation venography from MRI phase. MRM **72**(1), 149–159 (2014)
8. Lustig, M., Donoho, D., Pauly, J.M.: Sparse MRI: the application of compressed sensing for rapid MR imaging. MRM **58**(6), 1182–1195 (2007)
9. Liu, T., Spincemaille, P., de Rochefort, L., Kressler, B., Wang, Y.: Calculation of susceptibility through multiple orientation sampling (cosmos): a method for conditioning the inverse problem from measured magnetic field map to susceptibility source image in MRI. MRM **61**(1), 196–204 (2009)
10. Bilgic, B., Xie, L., Dibb, R., Langkammer, C., Mutluay, A., Ye, H., Polimeni, J.R., Augustinack, J., Liu, C., Wald, L.L., Setsompop, K.: Rapid multi-orientation quantitative susceptibility mapping. NeuroImage **125**, 1131–1141 (2016)
11. Li, W., Wu, B., Liu, C.: Quantitative susceptibility mapping of human brain reflects spatial variation in tissue composition. NeuroImage **55**(4), 1645–1656 (2011)
12. Schweser, F., Deistung, A., Lehr, B.W., Reichenbach, J.R.: Quantitative imaging of intrinsic magnetic tissue properties using MRI signal phase: an approach to in vivo brain iron metabolism. NeuroImage **54**(4), 2789–2807 (2011)
13. Smith, S.M.: Fast robust automated brain extraction. Hum. Brain Mapp. **17**(3), 143–155 (2002)
14. Toussaint, N., christophe Souplet, J., Fillard, P.: Medinria: medical image navigation and research tool by INRIA. In: Proceedings of MICCAI Workshop (2007)
15. Bremmer, J.P., Berckel, B.N.M., Persoon, S., Kappelle, L.J., Lammertsma, A.A., Kloet, R., Luurtsema, G., Rijbroek, A., Klijn, C.J.M., Boellaard, R.: Day-to-day test-retest variability of CBF, CMRO2, and OEF measurements using dynamic 15O pet studies. Mol. Imag. Biol. **13**(4), 759–768 (2010)